

Multi-color optical monitoring of the BL Lacertae object S5 0716+714 during the 2012 outburst

Shanwei Hong,

Yunnan Observatories, Chinese Academy of Sciences, 396 Yangfangwang, Guandu District,
Kunming, 650216, P. R. China

University of Chinese Academy of Sciences, Beijing 100049, China

Department of Mathematics and Computer Science, Lijiang Teachers College, Lijiang
674199, China

Dingrong Xiong and Jinming Bai

Yunnan Observatories, Chinese Academy of Sciences, 396 Yangfangwang, Guandu District,
Kunming, 650216, P. R. China

Center for Astronomical Mega-Science, Chinese Academy of Sciences, 20A Datun Road,
Chaoyang District, Beijing, 100012, P. R. China

Key Laboratory for the Structure and Evolution of Celestial Objects, Chinese Academy of
Sciences, 396 Yangfangwang, Guandu District, Kunming, 650216, P. R. China

xiongdongrong@ynao.ac.cn

Received _____; accepted _____

ABSTRACT

We have monitored the BL Lacertae object S5 0716+714 in the optical bands during 2012 January and February with long time spans on intraday timescales (>5 hr) and high time resolutions. During this monitoring period, the object shows violent flaring activity both in short and intraday timescales. The object has high value of duty cycle. The light curves detected as intraday variability (IDV) show variability of various shapes. The variability amplitude is from 12.81 per cent to 33.22 per cent, and the average value 19.92 ± 5.87 per cent. The overall magnitude variabilities are $\Delta B = 1^{\text{m}}.24$, $\Delta V = 1^{\text{m}}.42$, $\Delta R = 1^{\text{m}}.3$, $\Delta I = 1^{\text{m}}.23$ respectively. During the observations, the average change rate is $\langle CR \rangle = 0.035 \pm 0.009$ Mag/h during the ascent and $\langle CR \rangle = 0.035 \pm 0.014$ Mag/h during the descent. However, different cases are found on certain nights. There are good inter-bands correlations but not significant time lags for intraday and short timescales. The results of the autocorrelation function show that the variability timescales range from 0.054 day to 0.134 day. Most of nights show bluer when brighter (BWB) chromatic trend; a weak redder with brighter (RWB) trend is found; a few nights show no correlations between magnitude and color index. The BWB trend appears in the short timescales. During the flare the spectral index exhibits a clockwise loop for inter-nights. A shock-in-jet model and the shock wave propagating along a helical path are likely to explain the variability and color index variability.

Subject headings: BL Lacertae object: individual (S5 0716+714) - galaxies: active - galaxies: photometry

1. INTRODUCTION

BL Lacertae (BL Lac) objects are the most extreme subclass of active galactic nuclei (AGNs), hosted in massive elliptical galaxies, the emission of which is dominated by a relativistic jet closely aligned with the line of sight. This implies the existence of a parent population of sources with a misaligned jet that have been identified with low-power Fanaroff-Riley type I radio galaxies (FR Is). A most distinctive characteristic of the class is the weakness or absence of spectral lines that historically hindered the identification of their nature and ever thereafter proved to be a hurdle in the determination of their distance (Falomo et al. 2014; Angel & Stockman 1980; Urry & Padovani 1995). The spectrum of BL Lac objects, dominated by non-thermal emission over the whole electromagnetic range, together with bright compact radio cores, high luminosity, rapid and large amplitude flux variability at all frequencies and strong polarization make these sources become an optimal laboratory for high energy astrophysics. The broadband spectral energy distributions (SEDs) of BL Lac objects have a double peaked structure. The low energy peak at the IR-optical-UV band is explained with the synchrotron emission of relativistic electrons, and the high energy peak at the GeV-TeV gamma-ray band due to the inverse Compton (IC) scattering (e.g., Dermer et al. 1995; Dermer et al. 2002; Bottcher 2007). The hadronic model is an alternative explanation for the high energy emissions from BL Lac objects (e.g., Dermer et al. 2012). According to the difference of synchrotron peak frequency, BL Lac objects can be divided into low-synchrotron-peaked (LSP, $\nu_{\text{peak}}^s < 10^{14}\text{Hz}$), intermediate-synchrotron-peaked (ISP, $10^{14}\text{Hz} < \nu_{\text{peak}}^s < 10^{15}\text{Hz}$) and high-synchrotron-peaked (HSP, $10^{15}\text{Hz} < \nu_{\text{peak}}^s$) three categories (Abdo et al. 2010).

The variabilities of BL Lac objects at frequencies ranging from radio to TeV bands have been detected (e.g., Rani et al. 2013; Liao et al. 2014; Bartoli et al. 2016). The timescales of variabilities are from years down to minutes (e.g., Poon et al. 2009; Zhang et

al. 2008a; Fan et al. 2005, 2009a, 2014). Brightness changes of a few tenths or hundredths of a magnitude during hours or less are often known as intraday variability (IDV) or microvariability (Wagner & Witzel 1995). Short-term variability (STV) has timescales of days to weeks, even months, and long-term variability (LTV) ranges from months to years (Gupta et al. 2008a; Dai et al. 2015). IDV has been confirmed as intrinsic nature of the BL Lac objects and has become a subject of intense activity as its physical mechanisms are not understood well (e.g., Chandra et al. 2011; Fan et al. 2009b; Zhang et al. 2008b; Bai et al. 1998; Dai et al. 2015; Xiong et al. 2016). The shortest variability (microvariability) time-scales are important for understanding the geometry of jets, the magnetic field and black hole mass, because it provides a possible minimum size of variation sources (e.g., Gupta et al. 2009; Rani et al. 2010; Fan et al. 2009b, 2014; Zhang et al. 2008b; Dai et al. 2015; Xiong et al. 2016). The spectral index (or color behavior) is an important but a simple factor to explore the variability mechanism (e.g., Gu & Ai 2011; Zheng et al. 2008; Wu et al. 2007).

S5 0716+714 (R.A.=07^h21^m53^s.4, decl.=71°20′36″, J2000) is classified as an ISP BL Lac object ($\nu_{\text{peak}}^s = 10^{14.6}\text{Hz}$; Abdo et al. 2010). It was discovered in the Bonn-NRAO Radio Survey of flat-spectrum radio sources with a 4.9 GHz flux greater than 1 Jy (Kuehr et al. 1981). Radio maps detected a compact core-jet structure and an extended emission resembling an FR II object (Antonucci et al. 1986; Gabuzda et al. 1998). The source has a featureless optical continuum with the redshift 0.31 ± 0.08 derived by using the host galaxy as a standard candle (Nilsson et al. 2008). Danforth et al. (2013) used intervening absorption systems to set the redshift range $0.2315 < z < 0.3407$. It is one of the brightest BL Lac objects which is highly variable from the radio to γ -ray bands with very high duty cycle (Wagner & Witzel 1995). Because of its high power and lack of signs for ongoing accretion or surrounding gas, the source is an ideal candidate to explore the multi-wavelength non thermal emission. The flux and spectral variations of S5 0716+714

have been extensively studied over the entire electromagnetic spectrum (Wagner & Witzel 1995; Wagner et al. 1996; Heidt & Wagner 1996; Ghisellini et al. 1997; Sagar et al. 1999; Qian et al. 2002; Raiteri et al. 2003; Wu et al. 2005, 2007; Nesci et al. 2005; Gu et al. 2006; Montagni et al. 2006; Ostorero et al. 2006; Foschini et al. 2006; Zhang et al. 2008b; Villata et al. 2000, 2008; Gupta et al. 2008b, 2009, 2012; Vittorini et al. 2009; Stalin et al. 2006, 2009; Anderhub et al. 2009; Carini et al. 2011; Zhang et al. 2012; Hu et al. 2014; Dai et al. 2013; Larionov et al. 2013; Liao et al. 2014; Rani et al. 2010, 2014; Chandra et al. 2011, 2015; Dai et al. 2015; Bhatta et al. 2015, 2016; Wierzholska & Siejkowski 2015, 2016; Man et al. 2016; Agarwal et al. 2016; Li et al. 2017). From the observations of Poon et al. (2009), the object showed four fast flares with amplitudes ranging from 0.3 to 0.75 mag. Typical timescales of microvariability ranged from 2 to 8 hr. Strong bluer-when-brighter (BWB) chromatism was found on internight timescales. However, a different spectral behavior was found on intranight timescales. A possible time lag of ~ 11 minutes between B and I bands was found on one night. The observations from Chandra et al. (2011) suggested that S5 0716+714 showed night-to-night and intra-night variabilities at various time scales. Wu et al. (2007) found that the source showed two strong flares, with variation amplitudes of about 0.8 and 0.6 mag in the V band, respectively; strong BWB correlations were found for both internight and intranight variations; no apparent time lag was observed between the V and R band variations, and the observed BWB chromatism may be mainly attributed to the larger variation amplitude at shorter wavelength. Man et al. (2016) found that variations in the R and B bands were approximately 1.5 min lagging behind the I band for the object. But from results of Carini et al. (2011), there are no significant lags between the B and I -band flux variations. During nearly continuous multiband observations, Bhatta et al. (2016) presented that the source displayed pronounced variability and BWB spectral evolution. The results from Hu et al. (2014) showed a strong BWB trend on intranight time-scales and a mild bluer-when-brighter on internight time-scales for the source. Dai

et al. (2013) and Dai et al. (2015) found that BWB chromatism was observed in long, intermediate, and short timescales. Stalin et al. (2006) and Agarwal et al. (2016) found no evidence of spectral changes with the source brightness on either internight or intranight time-scales for the BL Lac object S5 0716+714 even when the target was in flaring state.

In order to further explore characteristics of IDV and STV timescales, and spectral properties on both intranight and internight timescales, we monitored the source in multi-color optical bands during the 2012 outburst. Due to the high temporal resolution and long time spans on intraday timescales, more accurate results can be obtained. This paper is organized as follows. The observations and data analysis are described in Section 2. Section 3 presents the results. Discussion and conclusions are reported in Section 4.

2. OBSERVATIONS AND DATA ANALYSIS

Our optical observations were carried out using a 60 cm BOOTES-4 auto-telescope which is located at the Lijiang Observatory of Yunnan Observatories of Chinese Academy of Sciences, where the longitude is $100^{\circ}01'51''$ E and the latitude $26^{\circ}42'32''$ N, with an altitude of 3193 m. Its main objective is to observe the gamma-ray bursts (GRBs) and blazars. Further details about the telescope are given in Table 1. During our observations, the telescope was equipped with standard Johnson UBV and Cousins RI filters. The optical observations in the B , V , R and I bands were in a corresponding cyclic mode. Time resolutions for most of nights are less than six minutes, and time spans on a night more than five hours (Table 2). The time intervals between V and R bands range from 30 s to 131 s, and most of nights have time intervals less than 50 s. The typical exposure times in the B , V , R and I bands are 60 s, 40 s, 40 s, 40 s respectively. So our observations with high temporal resolution (few minutes) can be considered as quasi-simultaneous measurements. All images have been prereduced with the CCDRED package, and then observing data were

processed using the photometric tool, DAOPHOT, in the IRAF¹ software package. The flat-field images were taken at dusk and dawn when possible. The bias images were taken at the beginning and the end of the observation. In order to determine aperture radius, we used different aperture radii ($1.5 \times \text{FWHM}$, $1.7 \times \text{FWHM}$, $2 \times \text{FWHM}$, $2.5 \times \text{FWHM}$, $3 \times \text{FWHM}$) to carry out aperture photometry for all observations on per night. We found less aperture radius with better mean S/N ratio on a night, i.e., $1.5 \times \text{FWHM}$ had the best mean S/N ratio on a night. Moreover, we plotted the aperture radii (from $1 \times \text{FWHM}$ to $4 \times \text{FWHM}$) versus magnitudes for different frames on a night. The results showed that the change rate of increasing brightness was rapid from $1 \times \text{FWHM}$ to $1.7 \times \text{FWHM}$, and quickly slow down after $1.7 \times \text{FWHM}$. When the aperture radius was near $3 \times \text{FWHM}$, the brightness almost kept constant. So considering the best S/N ratio and constant brightness, we made a compromise, i.e., the aperture radius of $1.7 \times \text{FWHM}$ was selected. In order to obtain pure skylight background, the target and other objects should be excluded from the sky annulus. The inner radius and width of sky annulus were $5 \times \text{FWHM}$ and $2 \times \text{FWHM}$ respectively. After correcting flat-field and bias, aperture photometry was performed, and then instrumental aperture magnitudes were obtained. The finding chart of S5 0716+714 was found in the webpage². From the above finding chart, we chose the marked 3 and 5 stars as comparison stars because their magnitudes were similar to that of the blazar, and the differential magnitude between 3 and 5 stars was the smallest variations among the comparison stars. Following Zhang et al. (2004, 2008a), Fan et al. (2014), Bai et al. (1998), the source magnitude was given as the average of the values derived with respect to the two comparison stars ($\frac{m_3+m_5}{2}$, m_3 was the blazar magnitude obtained from standard star 3 and m_5 from standard star 5). The magnitudes of comparison stars in the field of S5

¹IRAF is distributed by the National Optical Astronomy Observatories, which are operated by the Association of Universities for Research in Astronomy, Inc., under cooperative agreement with the National Science Foundation.

²<https://www.lsw.uni-heidelberg.de/projects/extragalactic/charts/0716+714.html>

0716+714 were taken from Villata et al. (1998) and Ghisellini et al. (1997). The observing uncertainty on each night was the rms error of the differential magnitude between two comparison stars. The rms errors of the photometry on a certain night were calculated from the two comparison stars, star 3 and star 5, in the usual way:

$$\sigma = \sqrt{\sum \frac{(m_i - \bar{m})^2}{N - 1}}, \quad i = 1, 2, 3, \dots, N, \quad (1)$$

where $m_i = (m_3 - m_5)_i$ is the differential magnitude of stars 3 and 5, while $\bar{m} = \overline{m_3 - m_5}$ is the averaged differential magnitude over the entire data set, and N is the number of the observations on a given night. The actual number of observations for S5 0716+714 is 13 nights obtaining 683 B -band, 871 V -band, 874 R -band and 878 I -band data points. The results of observations are given in Table 3 – 6 for filters B , V , R and I .

In order to quantify the IDV of the object, we have employed three statistical analysis techniques (C test, F test and the one-way analysis of variance (ANOVA); e.g., de Diego 2010; Goyal et al. 2012; Hu et al. 2014; Agarwal & Gupta 2015; Dai et al. 2015; Xiong et al. 2016). The blazar is considered as variability (V) if the light curve satisfies the three criteria of C -test, F -test and ANOVA. The blazar is considered as probably variable (PV) if only one of the above three criteria is satisfied. The blazar is considered as non-variable (N) if none of the criteria are met. Romero et al. (1999) introduced the variability parameter, C , as the average value between C_1 and C_2 :

$$C_1 = \frac{\sigma(BL - StarA)}{\sigma(StarA - StarB)}, C_2 = \frac{\sigma(BL - StarB)}{\sigma(StarA - StarB)}, \quad (2)$$

where (BL-StarA), (BL-StarB) and (StarA-StarB) are the differential instrumental magnitudes of the blazar and comparison star A, the blazar and comparison star B, and comparison stars A and B. σ is the standard deviation of the differential instrumental magnitudes. The adopted variability criterion requires $C \geq 2.576$, which corresponds to a 99 per cent confidence level. Despite the very common use of the C -statistics, de Diego

(2010) has pointed out that it has severe problems. The F -test is considered to be a proper statistics to quantify the IDV (e.g., de Diego 2010; Joshi et al. 2011; Goyal et al. 2012; Hu et al. 2014; Agarwal & Gupta 2015; Xiong et al. 2016). F value is calculated as

$$F_1 = \frac{Var(BL - StarA)}{Var(StarA - StarB)}, F_2 = \frac{Var(BL - StarB)}{Var(StarA - StarB)}, \quad (3)$$

where $Var(BL-StarA)$, $Var(BL-StarB)$ and $Var(StarA-StarB)$ are the variances of differential instrumental magnitudes. The F value from the average of F_1 and F_2 is compared with the critical F -value, $F_{\nu_{bl}, \nu_*}^\alpha$, where ν_{bl} and ν_* are the number of degrees of freedom for the blazar and comparison star respectively ($\nu = N - 1$), and α is the significance level set as 0.01 (2.6σ). If the average F value is larger than the critical value, the blazar is variable at a confidence level of 99 per cent. de Diego (2010) reported that the ANOVA is a powerful and robust estimator for microvariations. It does not rely on error measurement but derives the expected variance from subsamples of the data. The one-way ANOVA test divides the data into many groups. Then it compares the variances between inter-groups and intra-groups. From Appendix A3 of de Diego (2010), the statistics

$$F = \frac{\sum_{j=1}^k \sum_{i=1}^{n_j} (\bar{y}_j - \bar{y})^2 / (k - 1)}{\sum_{j=1}^k \sum_{i=1}^{n_j} (y_{ij} - \bar{y}_j)^2 / (N - k)} = \frac{SS_G / (k - 1)}{SS_R / (N - k)}, \quad (4)$$

where y_{ij} represents the i th observation (with $i = 1, 2, \dots, n_j$) on the j th group (with $j = 1, 2, \dots, k$), \bar{y} the mean of the whole data set, \bar{y}_j the mean on the j th group, k the number of groups, N the number of the whole data set. The SS_G and SS_R are between-groups sum of squares and within-groups sum of squares respectively. Considering the time of exposure, we bin the data in a group of five observations (see Xiong et al. 2016 and de Diego 2010 for detail). If the measurements in the last group are less than 5, then it is merged with the previous group. The critical value of ANOVA can be obtained by F_{ν_1, ν_2}^α in the F -statistics, where $\nu_1 = k - 1$, $\nu_2 = N - k$ and α is the significance level set as 0.01. if F value from equation (4) exceeds the critical value F_{ν_1, ν_2}^α , the blazar is variable at a confidence level of

99 per cent. In order to further quantify the reliability of variability, the value of S_x can be calculated as (e.g., Hu et al. 2014)

$$S_x = m_i - \overline{m}, \quad x = V, R, I, \quad (5)$$

where m_i and \overline{m} are same with equation (1). The variability amplitude (Amp) can be calculated by (Heidt & Wagner 1996)

$$\text{Amp} = 100 \times \sqrt{(A_{\max} - A_{\min})^2 - 2\sigma^2} \text{ percent}, \quad (6)$$

where A_{\max} and A_{\min} are the maximum and minimum magnitude, respectively, of the light curve for the night being considered, and σ is rms errors. When estimating the variability amplitude, we only consider the nights detected as variability.

The duty cycle (DC) is calculated as (Romero et al. 1999; Stalin et al. 2009; Hu et al. 2014)

$$\text{DC} = 100 \frac{\sum_{i=1}^n N_i (1/\Delta T_i)}{\sum_{i=1}^n (1/\Delta T_i)} \text{per cent}, \quad (7)$$

where $\Delta T_i = \Delta T_{i,obs}(1+z)^{-1}$, z is the redshift of the object and $\Delta T_{i,obs}$ is the duration of the monitoring session of the i th night. Note that since for a given source the monitoring durations on different nights were not always equal, the computation of DC has been weighted by the actual monitoring duration ΔT_i on the i th night. N_i will be set to 1 if intraday variability is detected, otherwise $N_i = 0$ (Goyal et al. 2013).

3. RESULTS

3.1. Variability

The analysis results on intraday variability are shown in Table 7. From Table 7, it can be seen that IDV is found on seven nights with at least two bands detected as IDV

on a night. The light curves detected as IDV are given in Fig. 1 which shows variability of various shapes. For the seven nights, we also check the color variations on intraday timescales. However, the results from three statistical tests do not show significant color variations on intraday timescales. The rest of nights are considered as PV except for the I band on February 6. Generally, On January 27, the brightness first increases and then decreases along the arc. On January 28, the brightness first increases and then decreases, and last increases. On January 29, the brightness first decreases and then increases along the symmetrical arc. On January 30, the brightness changes are similar with that on January 29 but not along the symmetrical arc. On February 1 and 8, the brightness continues to increase while on February 4, the brightness continues to decrease. The corresponding changes of magnitude and change rate are seen in Table 8. When calculating the change rate, we first determine increasing or decreasing time points and then use the slope from errors weighted linear regression analysis as change rate. The results from Table 8 show that the average change rate is $\langle CR \rangle = 0.035 \pm 0.009$ Mag/h during the ascent and $\langle CR \rangle = 0.035 \pm 0.014$ Mag/h during the descent. The average change rates between the ascent and descent are equal. However, different cases are found on certain nights. The corresponding times of variation range from 47 min to 274 min. On January 29, the increasing and decreasing change rates are close. The correlations between variability amplitude and the source average brightness are shown in Fig. 2. Although Fig. 2 shows trends/tendencies of larger amplitude with brighter magnitude for I and R bands, the analysis of non-parametric Spearman rank indicates that there are not significant correlations between variability amplitude and the source average brightness for different wavebands (significance level $P_I = 0.1$, $P_R = 0.1$, $P_V = 0.8$, $P_B = 0.7$). The variability amplitude is from 12.81 per cent to 33.22 per cent, and the average value 19.92 ± 5.87 per cent (Table 7 and Fig. 2). Making use of equation (6), we calculate DC of intraday variability. The value of DC is 44% for S5 0716+714 (98%, if PV cases are also included).

Short-term light curves and color index are given in Fig. 3. From Fig. 3, we can see that on the whole the BL Lac object continues to brighten with a remarkably first brightening and then darkening peak during the short term, and the average color index on each night remains approximately constant during this period. The overall magnitude variabilities are $\Delta B = 1^m.24$, $\Delta V = 1^m.42$, $\Delta R = 1^m.3$, $\Delta I = 1^m.23$ respectively. The magnitude distributions in the B , V , R and I bands are $14^m.89 < B < 13^m.65$, $14^m.45 < V < 13^m.03$, $13^m.94 < R < 12^m.64$ and $13^m.39 < I < 12^m.16$ respectively. The average values of magnitude and color index are $\langle B \rangle = 14^m.35 \pm 0^m.31$, $\langle V \rangle = 13^m.73 \pm 0^m.36$, $\langle R \rangle = 13^m.33 \pm 0^m.34$, $\langle I \rangle = 12^m.81 \pm 0^m.33$ and $\langle V - R \rangle = 0^m.39 \pm 0^m.04$ respectively.

3.2. Cross-correlation Analysis and Variability Timescales

Following Giveon et al. (1999), Wu et al. (2007), Liu et al. (2008), Liao et al. (2014) and Xiong et al. (2016), we use the z -transformed discrete correlation function (ZDCF; Alexander 1997) to perform the inter-bands correlation analysis and search for the possible inter-bands time delay. The ZDCF code of Alexander et al. (1997) can automatically set how many bins are given, and be used to calculate the inter-bands correlation and the ACF. In order to achieve statistical significance, the minimal number of points per bin is 10. The results of ZDCF for all data are given in Fig. 4. As an illustration, the results of ZDCF on four nights are given in Fig. 4. The results of ZDCF show that there are good inter-bands correlations but not significant time lags.

The zero-crossing time of the autocorrelation function (ACF) is a well-defined quantity and used as a characteristic variability timescale (e.g., Alexander 1997; Giveon et al. 1999; Netzer et al. 1996; Liu et al. 2008). The zero-crossing time is the shortest time it takes the ACF to fall to zero (Alexander 1997). If there is an underlying signal in the light curve, with

a typical timescale, then the width of the ACF peak near zero time lag will be proportional to this timescale (Giveon et al. 1999; Liu et al. 2008). The width of the ACF may be related to a characteristic size scale of the corresponding emission region (Chatterjee et al. 2012). Another function used in variability studies to estimate the variability timescales is the first-order structure function (SF; e.g., Trevese et al. 1994). There is a simple relation between the ACF and the SF (Giveon et al. 1999). We therefore perform only an ACF analysis on our lightcurves. The ACF was estimated by ZDCF. We only analyze the nights detected as intraday variability. The results of ACF analysis are given in Fig. 5. The results of ACF analysis on February 04 and 08 are not shown in Fig. 5 because all of the ACF values of the two nights are more than zero. Following Giveon et al. (1999), we then use a least-squares procedure to fit a fifth-order polynomial to the ACF, with the constraint that $\text{ACF}(\tau = 0) = 1$. From the fitting results, it is seen that the variability timescales range from 0.054 day to 0.134 day.

3.3. Correlation between Magnitude and Color Index

For the color index, we used the correction factors from Schlafly & Finkbeiner (2011) to correct the Galactic extinction. In order to minimize the bias introduced by the dependence of the color index on the magnitudes, brightness was calculated by averaging the magnitudes of the two bands used to calculate the index (Dai et al. 2015). We concentrate on $V - R$ index and $(V + R)/2$ magnitude because $V - R$ index is frequently studied. Fig. 6 shows the correlations between $V - R$ index and $(V + R)/2$ magnitude on intraday and short timescales. The results of analysis of Spearman rank are given in Table 9. The Table 9 shows that 8 nights have the significant correlations between $V - R$ index and $(V + R)/2$ magnitude, and 1 night has significant anti-correlation between $V - R$ index and $(V + R)/2$ magnitude (significance level $P < 0.05$ confidence level). Moreover, 4 nights have not

significant correlations between $V - R$ index and $(V + R)/2$ magnitude ($P > 0.05$). For short timescales, the significant correlation between $V - R$ index and $(V + R)/2$ magnitude is found (Table 9). Therefore, during the outburst period, most of nights show bluer when brighter (BWB) chromatic trend; a weak redder with brighter (RWB) trend is found; a few nights show no correlations between magnitude and color index. The BWB trend appears in the short timescales. The spectral index versus the flux in the flare event is given in Fig. 7. It is seen that during the flare the spectral index exhibits a clockwise loop for inter-nights.

4. DISCUSSION AND CONCLUSIONS

4.1. Variability

We have observed the BL Lac object S5 0716+714 with long time spans on intraday timescale (>5 hr) and high time resolutions. During this monitoring period, the object shows violent flaring activity both in short term and intraday timescales. The value of DC is 44% for S5 0716+714 (98%, if PV cases are also included). If we only consider the F test and ANOVA, the value of DC is 74%. So, similar to the previous results (e.g., Agarwal et al. 2016; Hu et al. 2014; Chandra et al. 2011; Stalin et al. 2009), the object has high value of DC. The light curves detected as IDV show variability of various shapes. The variability amplitude is from 12.81 per cent to 33.22 per cent, and the average value 19.92 ± 5.87 per cent. The overall magnitude variabilities are $\Delta B = 1^m.24$, $\Delta V = 1^m.42$, $\Delta R = 1^m.3$, $\Delta I = 1^m.23$ respectively. During the observations, the average change rate is $\langle CR \rangle = 0.035 \pm 0.009$ Mag/h during the ascent and $\langle CR \rangle = 0.035 \pm 0.014$ Mag/h during the descent, i.e., the average change rates between the ascent and descent are equal. However, different cases are found on certain nights. On January 29, the brightness first decreases and then increases along the symmetrical arc. Also the increasing and decreasing change rates are close on the night. From previous observations (Agarwal et al. 2016; Man

et al. 2016; Dai et al. 2015; Hu et al. 2014; Wu et al. 2007, 2012; Chandra et al. 2011; Stalin et al. 2009; Poon et al. 2009; Sasada et al. 2008; Zhang et al. 2008b;), many of the common cases of variability in the object are as follows: (i) the brightness continues to increase/decrease; (ii) the brightness first decreases and then increases, or vice versa, but not along the symmetrical arc; (iii) the brightness first increases and then decreases, and last increases; (iv) the brightness first increases and then decreases along the arc. These cases of variability have also been found in Fig. 1. Compared with these cases of variability, the type of variability on January 29 is rarely found on intraday timescales. From Fig. 3, we can obtain that the brightness is likely to increase from January 28 to January 29, and then decrease from January 29 to January 30. In addition, the color index on January 29 has BWB trend. Therefore, the variability on the night is likely related with relativistic jet activities (also see the following discussions).

For blazar, these components (jet, accretion disk and host galaxy) could contribute the emission of optical band. The host galaxy is more than 4 mag fainter than the brightness of S5 0716+714 (Nilsson et al. 2008). During the outburst period, the accretion disk radiation is always overwhelmed by the Doppler boosting flux from the relativistic jet. Then the variability of S5 0716+714 in the outburst state is likely to have an association with jet activities. The shock-in-jet model is often used to explain the IDV/short variability. The shocks propagate down relativistic jets, sweeping emitting regions. If the emitting regions have intrinsic variations (magnetic field, particle velocity/distribution, a large number of new particles injected), then we could see the IDV/short variability (Marscher & Gear 1985; Xiong et al. 2017). In addition to intrinsic variations, geometrical variations also could bring in flux variations. Rani et al. (2015) presented a high-frequency very long baseline interferometry (VLBI) kinematical study of the BL Lac object S5 0716+714. They found repetitive optical/ γ -ray flares and the curved trajectories of the associated components, and suggested that the shock front propagates along a bent trajectory or helical path.

In order to explain the multi-frequency behavior of an optical- γ -ray outburst in 2011, Larionov et al. (2013) also suggest a shock wave propagating along a helical path in the blazars jet. The helical jet structure may cause the Doppler factor change on a very short variability timescale (Gopal-Krishna & Wiita 1992). The variability may also be explained by turbulence behind an outgoing shock along the jet or the magnetic reconnections (Agarwal et al. 2016; Chandra et al. 2015). The symmetric/asymmetric light curves can be interpreted as arising from light-travel time effect (Chiaberge & Ghisellini 1999; Chatterjee et al. 2012). Chiaberge & Ghisellini (1999) presented that the symmetric shapes of the light curves strongly constrain the injection and cooling timescales. When the cooling time of the electrons is much shorter than the light crossing time, the light curves are symmetric. When the cooling time of the electrons is much larger than the light crossing time, the light curves are asymmetric.

The results of ACF show that the variability timescales range from 0.054 day to 0.134 day. If we consider the variability timescales as the light crossing time of the emitting blob, the range of the emission region in the jet is from $R \leq 2.14 \times 10^{15}$ cm to $R \leq 5.3 \times 10^{15}$ cm ($R \leq c\delta\Delta t_{min}/(1+z)$, where $\delta = 20$ from Nesci et al. (2005) and the redshift $z = 0.31$). In addition, there are good inter-bands correlations but not significant time lags for intraday and short timescales, and not significant correlations between variability amplitude and the source average brightness at individual bands. However, we still need more data to further confirm the correlations between variability amplitude and the source average brightness at individual bands due to the small sample size at individual bands in this work.

4.2. Spectral Properties

Generally, the BWB (bluer when brighter) chromatic trend is dominant for most of blazars while redder when brighter (RWB) trend is also found, especially for FSRQ (e.g.,

Gu et al. 2006; Guo & Gu 2016). The BWB behavior is most likely to be explained by the shock-in-jet model. According to the shock-in-jet model, as the shock propagating down the jet strikes a region with a large electron population, radiations at different visible colors are produced at different distances behind the shocks. High-energy photons from the synchrotron mechanism typically emerge sooner and closer to the shock front than the lower frequency radiation, thus causing color variations (Agarwal & Gupta 2015; Xiong et al. 2017). The BWB trend could be explained by two different jet components, i.e., flare component has a higher synchrotron peak frequency than the underlying component (Ikejiri et al. 2011). Assuming that the optical/UV variability is triggered by fluctuations, Guo & Gu (2016) presented that the RWB trend can likely be explained if the fluctuations occur first in the outer disk region, and the inner disk region has not yet fully responded when the fluctuations are being propagated inward. In contrast, the common BWB trend implies that the fluctuations likely more often happen first in the inner disk region. Gu et al. (2006) proposed that the different relative contributions of the thermal versus non-thermal radiation to the optical emission may be responsible for the different trends of the colour index with brightness in FSRQs and BL Lac objects. Moreover, the achromatic trend could be due to a Doppler factor variation on a spectrum slightly deviating from a power law (Villata et al. 2004). For our results, the average color index on each night remains approximately constant during this period. Most of nights show bluer when brighter (BWB) chromatic trend; a weak redder with brighter (RWB) trend is found; a few nights show no correlations between magnitude and color index. The BWB trend appears in the short timescales. As discussed above, the variability and color index of S5 0716+714 in the outburst state are likely to have an association with jet activities. The shock-in-jet model can explain the BWB chromatic trend. The BWB or flatter when brighter could be due to the injection of fresh electrons, with an energy distribution harder than that of the previous cooled ones (e.g., Kirk et al. 1998; Mastichiadis & Kirk 2002). However, if

the injection of fresh electrons have an energy distribution softer than that of the previous cooled ones, the weak RWB may be seen. When a shock wave propagates along a helical path, the achromatic trend could be found. Therefore, a shock-in-jet model and the shock wave propagating along a helical path are likely to explain the variability and color index variability.

Finally, during the flare the spectral index exhibits a clockwise loop for inter-nights. This type of variability pattern represents a sort of hysteresis cycle in the scatter plot between the energy index and the flux. It may arise whenever the spectral slope is controlled by cooling processes (Fiorucci et al. 2004). The clockwise direction is due to changes in the injection of accelerated particles, propagating from high to low energies (Kirk et al. 1998).

We sincerely thank the referee for valuable comments and suggestions. We acknowledge the support of the staff of the Lijiang 2.4m and BOOTES-4 telescopes. Funding for the two telescopes has been provided by the Chinese Academy of Sciences and the Peoples Government of Yunnan Province. This work is financially supported by the National Nature Science Foundation of China (11433004, 11133006, 11673057, 11361140347), the Key Research Program of the Chinese Academy of Sciences (grant No. KJZD-EW-M06), the Strategic Priority Research Program “The emergence of Cosmological Structures” of the Chinese Academy of Sciences (grant No. XDB09000000), the Chinese Western Young Scholars Program and the Light of West China Program provided by CAS (Y7XB018001, Y5XB091001), the science and technology project for youth of Yunnan of China (2104FD059). This research has made use of the NASA/IPAC Extragalactic Database (NED), that is operated by Jet Propulsion Laboratory, California Institute of Technology, under contract with the National Aeronautics and Space Administration.

REFERENCES

- Abdo, A. A., Ackermann, M., Agudo, I., et al. 2010, *ApJ*, 716, 30
- Agarwal, A., & Gupta, A. C. 2015, *MNRAS*, 450, 541
- Agarwal, A., Gupta, A. C., Bachev, R., et al. 2016, *MNRAS*, 455, 680
- Alexander, T. 1997, in *Astronomical Time Series*, ed. D. Maoz, A. Sternberg, & E. M. Leibowitz (Dordrecht: Kluwer), 163
- Anderhub, H., Antonelli, L. A., Antoranz, P., et al. 2009, *ApJ*, 704, 129
- Angel, J. R. P., & Stockman, H. S. 1980, *ARA&A*, 18, 321
- Antonucci, R. R. J., Hickson, P., Olszewski, E. W., & Miller, J. S. 1986, *AJ*, 92, 1
- Bai, J. M., Xie, G. Z., Li, K. H., Zhang, X., & Liu, W. W. 1998, *A&AS*, 132, 83
- Bartoli, B., Bernardini, P., Bi, X. J., et al. 2016, *ApJS*, 222, 6
- Bhatta, G., Goyal, A., Ostrowski, M., et al. 2015, *ApJ*, 809, 27
- Bhatta, G., Stawarz, L., Ostrowski, M., et al. 2016, *ApJ*, 831, 92
- Bottcher, M. 2007, *Ap&SS*, 309, 95
- Carini, M. T., Walters, R., & Hopper, L. 2011, *AJ*, 141, 49
- Chandra, S., Baliyan, K. S., Ganesh, S., & Joshi, U. C. 2011, *ApJ*, 731, 118
- Chandra, S., Zhang, H., Baliyan, K. S., et al. 2015, *ApJ*, 809, 130
- Chatterjee, R., Bailyn, C. D., Bonning, E. W., et al. 2012, *ApJ*, 749, 191
- Chiaberge, M., & Ghisellini, G. 1999, *MNRAS*, 306, 551

- Dai, B. Z., Zeng, W., Jiang, Z. J., et al. 2015, *ApJS*, 218, 18
- Dai, Y., Wu, J. H., Zhu, Z. H., et al. 2013, *ApJS*, 204, 22
- Danforth, C. W., Nalewajko, K., France, K., Keeney, B. A. 2013, *ApJ*, 764, 57
- de Diego, J. A. 2010, *AJ*, 139, 1269
- Dermer, C. D. 1995, *ApJ*, 446, 63
- Dermer, C. D., & Schlickeiser, R. 2002, *ApJ*, 575, 667
- Falomo, R., Pian, E., & Treves, A. 2014, *A&A Rev.*, 22, 73
- Fan, J. H. 2005, *ChJAA*, 5, 213
- Fan, J. H., Peng, Q. S., Tao, J., Qian, B. C., & Shen, Z. Q. 2009a, *AJ*, 138, 1428
- Fan, J. H., Zhang, Y. W., Qian, B. C., et al. 2009b, *ApJS*, 181, 466
- Fan, J. H., Kurtanidze, O., Liu, Y., et al. 2014, *ApJS*, 213, 26
- Fiorucci, M., Ciprini, S., & Tosti, G. 2004, *A&A*, 419, 25
- Foschini, L., et al. 2006, *A&A*, 455, 871
- Gabuzda, D. C., Kovalev, Y. Y., Krichbaum, T. P., et al. 1998, *A&A*, 333, 445
- Ghisellini, G., et al. 1997, *A&A*, 327, 61
- Giveon, U., Maoz, D., Kaspi, S., Netzer, H., Smith, P. S. 1999, *MNRAS*, 306, 637
- Gopal-Krishna, Wiita, P. J. 1992, *A&A*, 259, 109
- Goyal, A., Gopal-Krishna, Wiita, P. J., Anupama, G. C., et al. 2012, *A&A*, 544, 37
- Goyal, A., Gopal-Krishna, Wiita, P. J., Stalin, C. S., & Sagar, R. 2013, *MNRAS*, 435, 1300

- Gu, M. F., Lee, C. U., Pak, S., Yim, H. S. & Fletcher, A. B. 2006, *A&A*, 459, 39
- Gu, M. F., & Ai, Y. L. 2011, *A&A*, 528, 95
- Guo, H. X., & Gu, M. F. 2016, *ApJ*, 822, 26
- Gupta, A. C., Deng, W. G., Joshi, U. C., Bai, J. M., & Lee, M. G. 2008a, *New A*, 13, 375
- Gupta, A. C., Fan, J. H., Bai, J. M., & Wagner, S. J. 2008b, *AJ*, 135, 1384
- Gupta, A. C., Srivastava, A. K., Wiita, P. J. 2009, *ApJ*, 690, 216
- Gupta, A. C., Krichbaum, T. P., Wiita, P. J. *MNRAS*, 2012, 425, 1357
- Heidt, J., & Wagner, S. J. 1996, *A&A*, 305, 42
- Hu, S. M., Chen, X., Guo, D. F., Jiang, Y. G., & Li, K. 2014, *MNRAS*, 443, 2940
- Ikejiri, Y., Uemura, M., Sasada, M., et al. 2011, *PASJ*, 63, 639
- Joshi, R., Chand, H., Gupta, A. C., & Wiita, P. J. 2011, *MNRAS*, 412, 2717
- Kirk, J. G., Rieger, F. M., & Mastichiadis, A. 1998, *A&A*, 333, 452
- Kuehr, H., Pauliny-Toth, I. I. K., Witzel, A., & Schmidt, J. 1981, *AJ*, 86, 854
- Larionov, V. M., Jorstad, S. G., Marscher, A. P., et al. 2013, *ApJ*, 768, 40
- Li, Y. T., Hu, S. M., Jiang, Y. G., et al. 2017, *PASP*, 129, 014101
- Liao, N. H., Bai, J. M., Liu, H. T., et al. 2014, *ApJ*, 783, 83
- Liu, H. T., Bai, J. M., Zhao, X. H., & Ma, L. 2008, *ApJ*, 677, 884
- Man, Z., Zhang, X., Wu, J., Yuan, Q. 2016, *MNRAS*, 456, 3168
- Marscher, A. P., & Gear, W. K. 1985, *ApJ*, 298, 114

- Mastichiadis, A., & Kirk, J. G. 2002, *PASA*, 19, 138
- Montagni, F., Maselli, A., Massaro, E., et al. 2006, *A&A*, 451, 435
- Nesci, R., Massaro, E., Rossi, C., et al. 2005, *AJ*, 130, 1466
- Netzer, H., Heller, A., Loinger, F., et al. 1996, *MNRAS*, 279, 429
- Nilsson, K., Pursimo, T., Sillanpaa, A., Takalo, L. O., & Lindfors, E. 2008, *A&A*, 487, 29
- Ostorero, L., et al. 2006, *A&A*, 451, 797
- Poon, H., Fan, J. H., & Fu, J. N. 2009, *ApJS*, 185, 511
- Raiteri, C. M., et al. 2003, *A&A*, 402, 151
- Rani, B., Gupta, A. C., Joshi, U. C., Ganesh, S., & Wiita, P. J. 2010, *ApJ*, 719, 153
- Rani, B., Krichbaum, T. P., Fuhrmann, L., et al. 2013, *A&A*, 552, 11
- Rani, B., Krichbaum, T. P., Marscher, A. P., et al. 2014, *A&A*, 571, 2
- Rani, B., Krichbaum, T. P., Marscher, A. P., et al. 2015, *A&A*, 578, 123
- Romero, G. E., Cellone, S. A., & Combi, J. A. 1999, *A&AS*, 135, 477
- Qian, B., Tao, J., & Fan, J. H. 2002, *AJ*, 123, 678
- Sagar, R., Gopal-Krishna, Mohan, V., Pandey, A. K., Bhatt, B. C., & Wagner, S. J. 1999, *A&AS*, 134, 453
- Sasada, M., Uemura, M., Arai, A., et al. 2008, *PASJ*, 60, 37
- Schlaafy, E. F., & Finkbeiner, D. P. 2011, *ApJ*, 737, 103
- Stalin, C. S., Gopal-Krishna, Sagar, R., Wiita, P. J., Mohan, V., & Pandey, A. K. 2006, *MNRAS*, 366, 1337

- Stalin, C. S., Kawabata, K. S., Uemura, M., et al. 2009, MNRAS, 399, 1357
- Trevese, D., Kron, R. G., Majewski, S. R., Bershady, M. A., & Koo, D. C. 1994, ApJ, 433, 494
- Urry, C. M., & Padovani, P. 1995, PASP, 107, 803
- Villata, M., Raiteri, C. M., Lanteri, L., Sobrito, G., & Cavallone, M. 1998, A&AS, 130, 305
- Villata, M., et al. 2000, A&A, 363, 108
- Villata, M., et al. 2008, A&A, 481, L79
- Villata, M., Raiteri, C. M., Kurtanidze, O. M., et al. 2004, A&A, 421, 103
- Vittorini, V., Tavani, M., Paggi, A., et al. 2009, ApJ, 706, 1433
- Wagner, S. J., & Witzel, A. 1995, ARA&A, 33, 163
- Wagner, S. J., et al. 1996, AJ, 111, 2187
- Wiercholska, A., & Siejkowski, H. 2015, MNRAS, 452, 11
- Wiercholska, A., & Siejkowski, H. 2016, MNRAS, 458, 2350
- Wu, J., Peng, B., Zhou, X., et al. 2005, AJ, 129, 1818
- Wu, J., Zhou, X., Ma, J., et al. 2007, AJ, 133, 1599
- Xiong, D. R., Zhang, H. J., Zhang, X., et al. 2016, ApJS, 222, 24
- Xiong, D. R., Bai, J. M., Zhang, H. J., et al. 2017, ApJS, 229, 21
- Zhang, B. K., Dai, B. Z., Wang, L. P., et al. 2012, MNRAS, 421, 3111
- Zhang, X., Zhang, L., Zhao, G., Xie, Z. H., Wu, L., & Zheng, Y. G. 2004, AJ, 128, 1929

Zhang, X., Zheng, Y. G., Zhang, H. J., & Hu, S. M. 2008a, ApJS, 174, 111

Zhang, X., Zheng, Y. G., Zhang, H. J., & Hu, S. M. 2008b, AJ, 136, 1846

Zheng, Y. G., Zhang, X., Bi, X. W., Hao, J. M., & Zhang, H. J. 2008, MNRAS, 385, 823

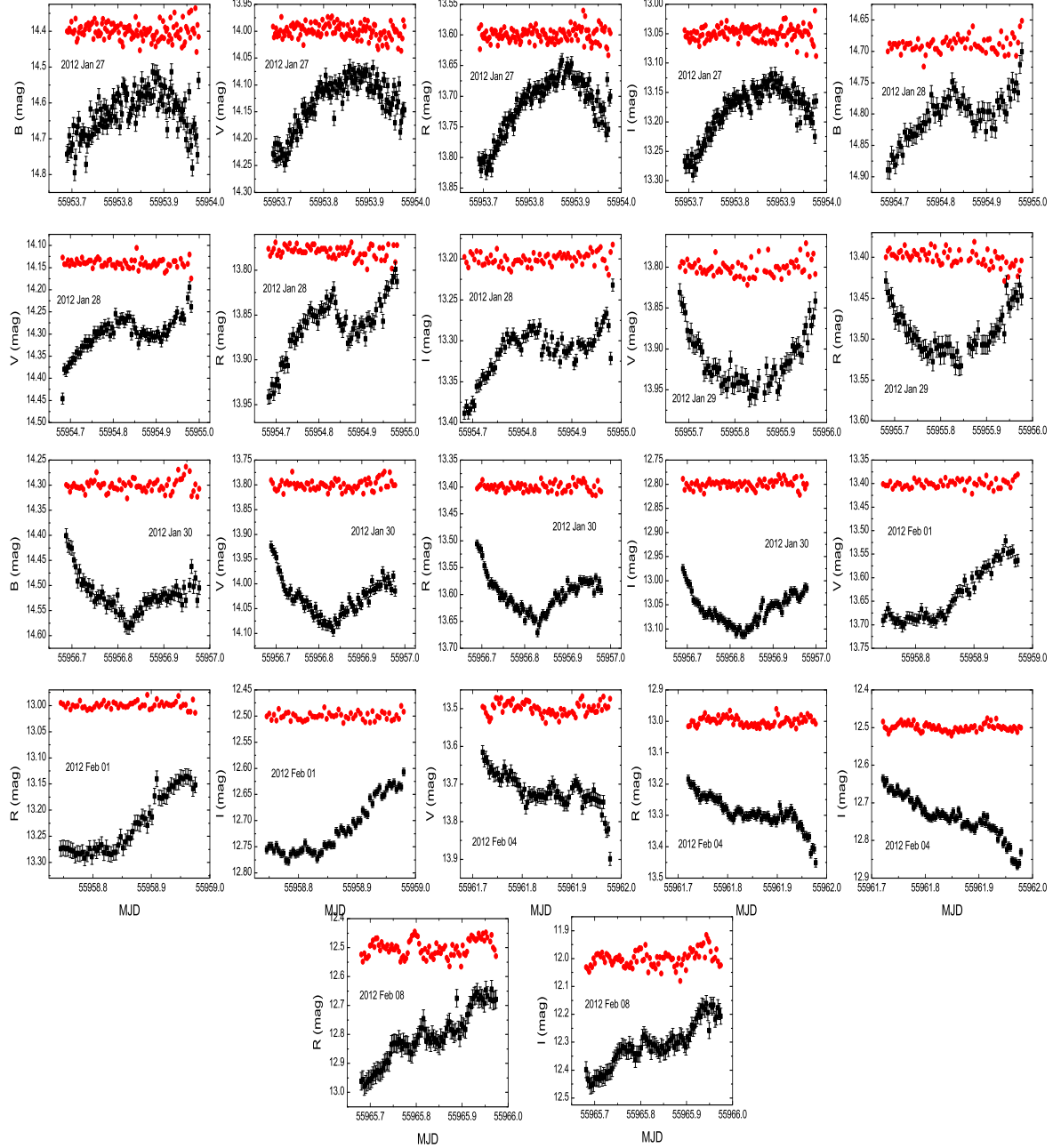


Fig. 1.— Light curves of intraday variability for S5 0716+714. The black squares are the light curves for S5 0716+714. The red circles are the variations of S_I , S_R , S_V and S_B . The light curves of S_I , S_R , S_V and S_B are offset to avoid their eclipsing with light curves of S5 0716+714.

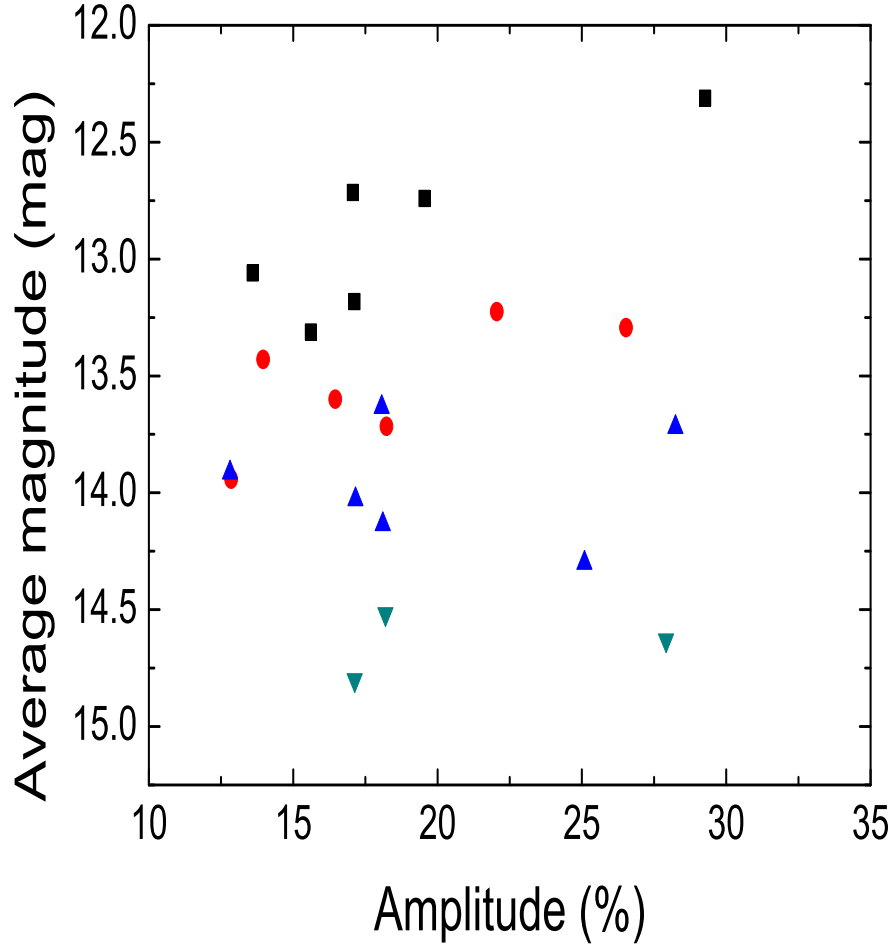


Fig. 2.— The variability amplitude versus the average brightness. Different symbols stand for different optical bands. The black rectangles stand for *I* band, red circles for *R* band, positive triangles for *V* band and anti-triangles for *B* band.

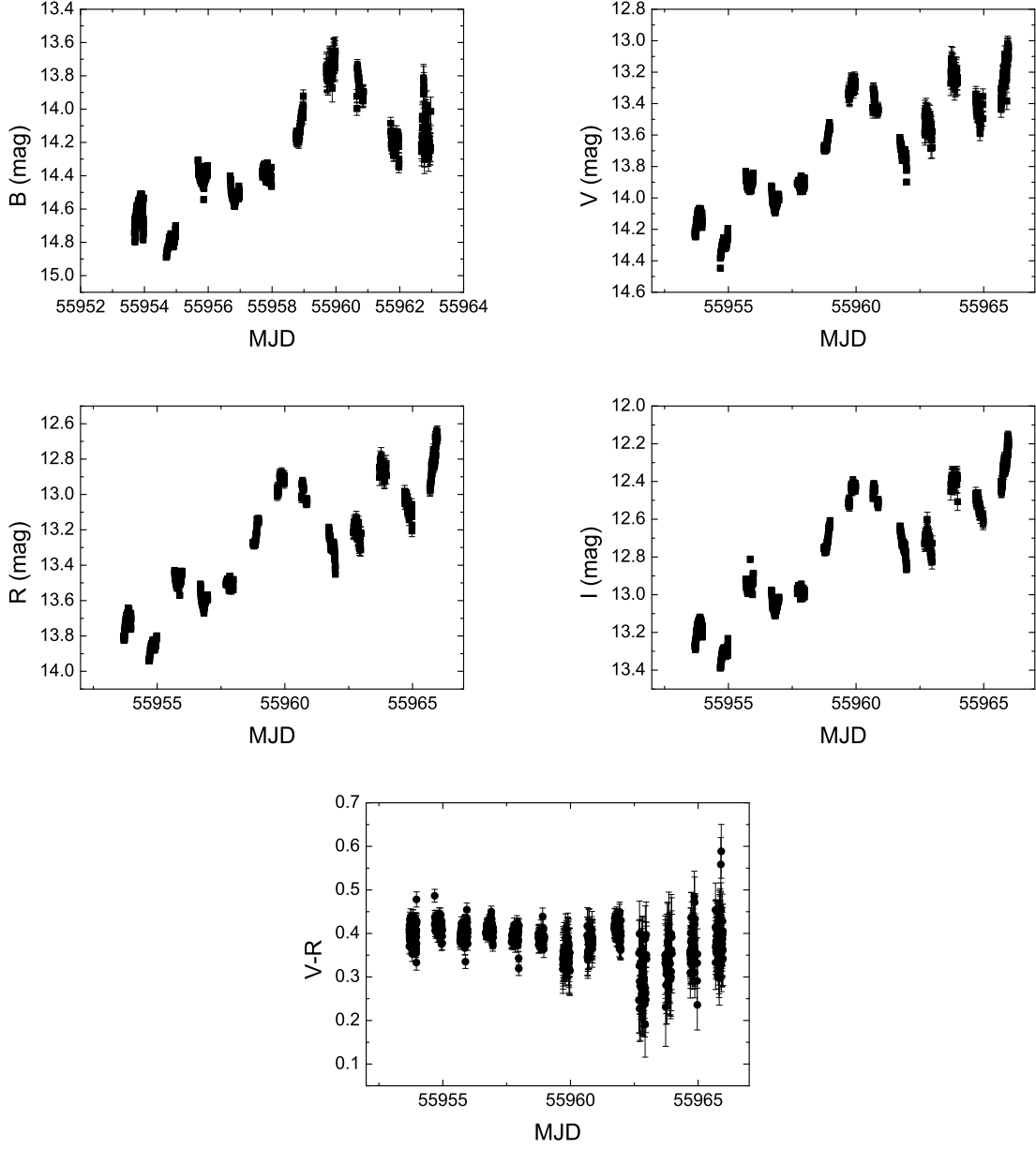


Fig. 3.— Short-term light curves of S5 0716+714 in B , V , R and I bands and color index $V - R$.

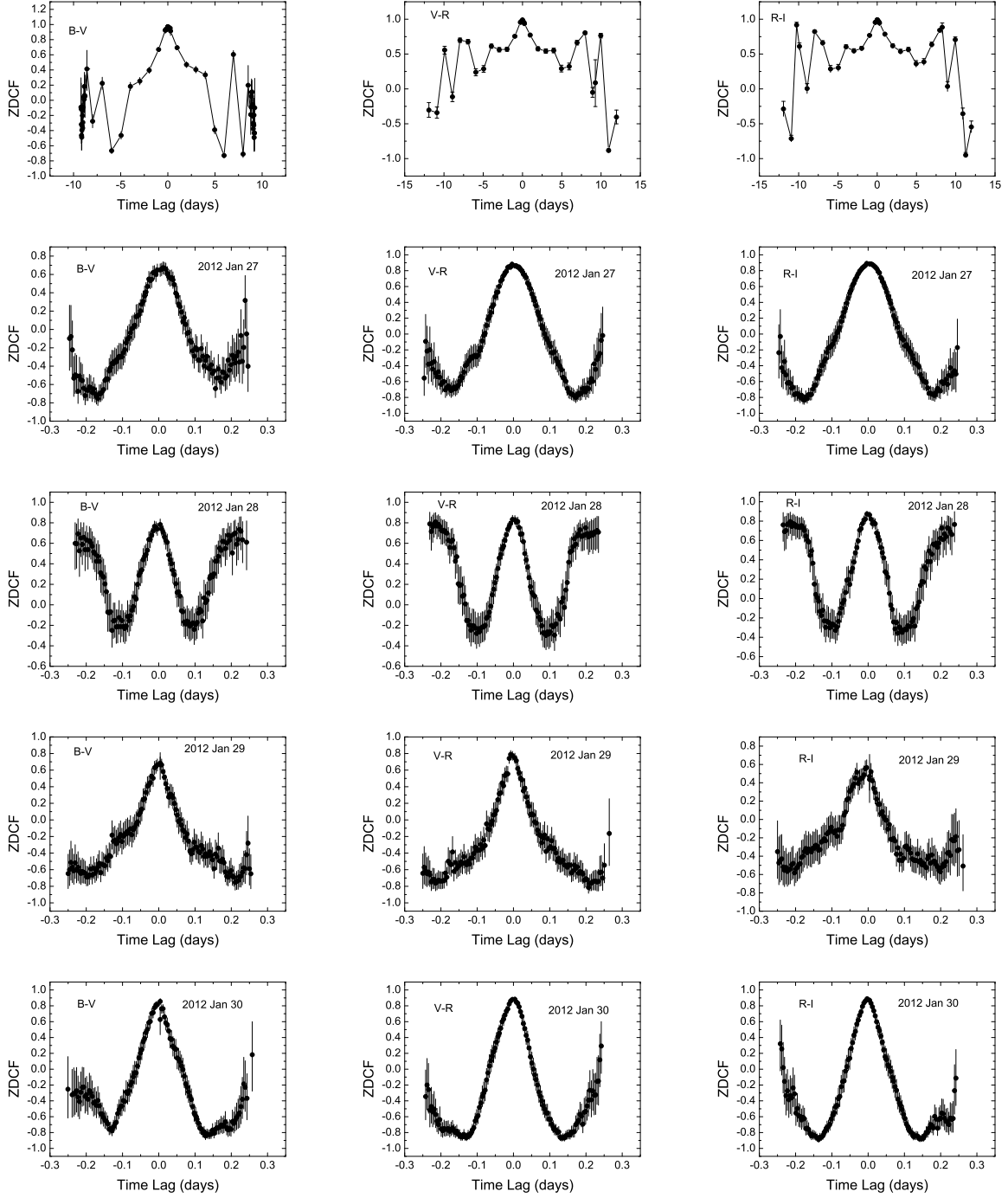


Fig. 4.— The ZDCF plots. The first panel is the results of ZDCF for all data. The rest of panels are the results of ZDCF for intraday timescales.

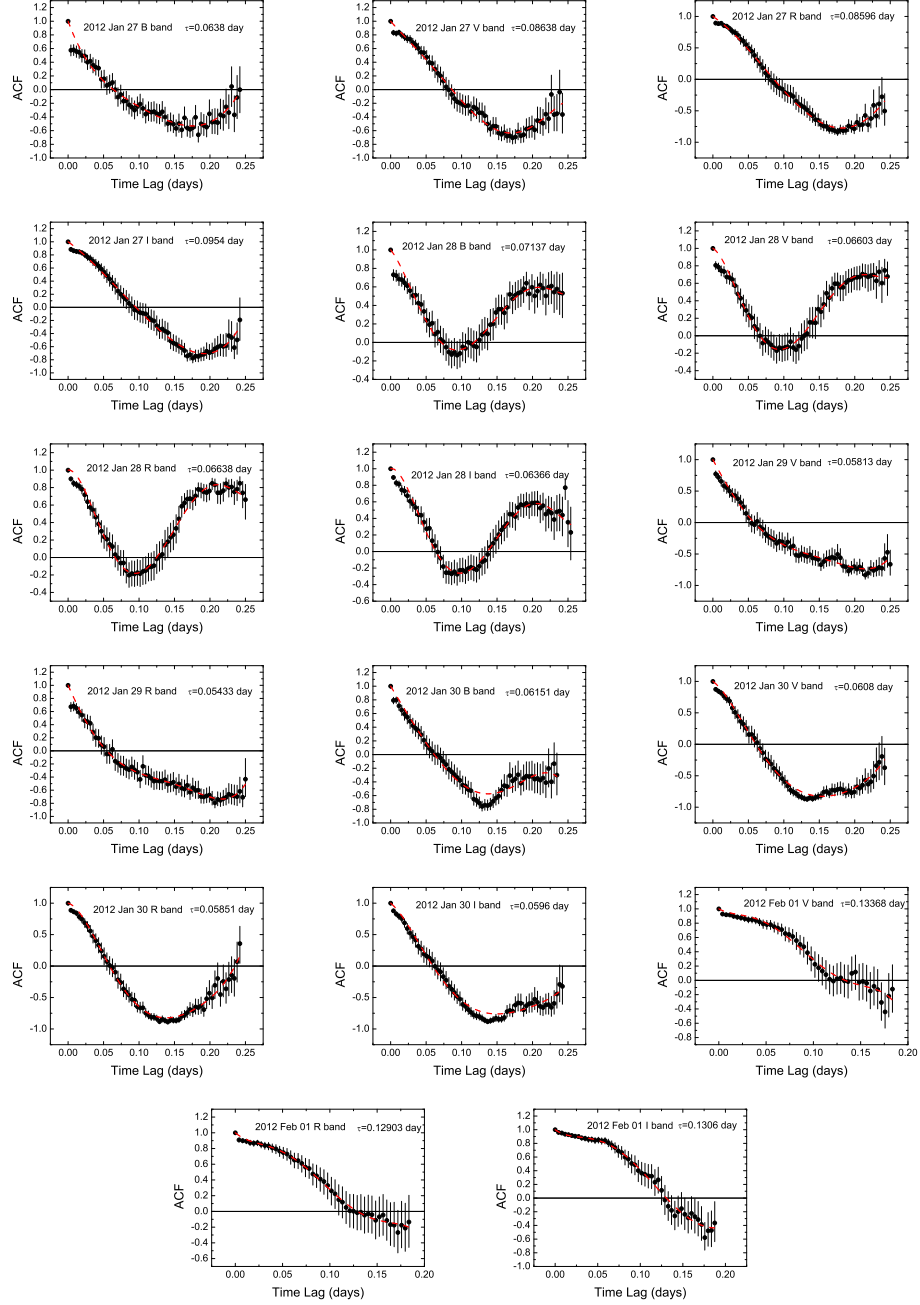


Fig. 5.— The results of ACF analysis. The red dashed line is a fifth-order polynomial least-squares fit.

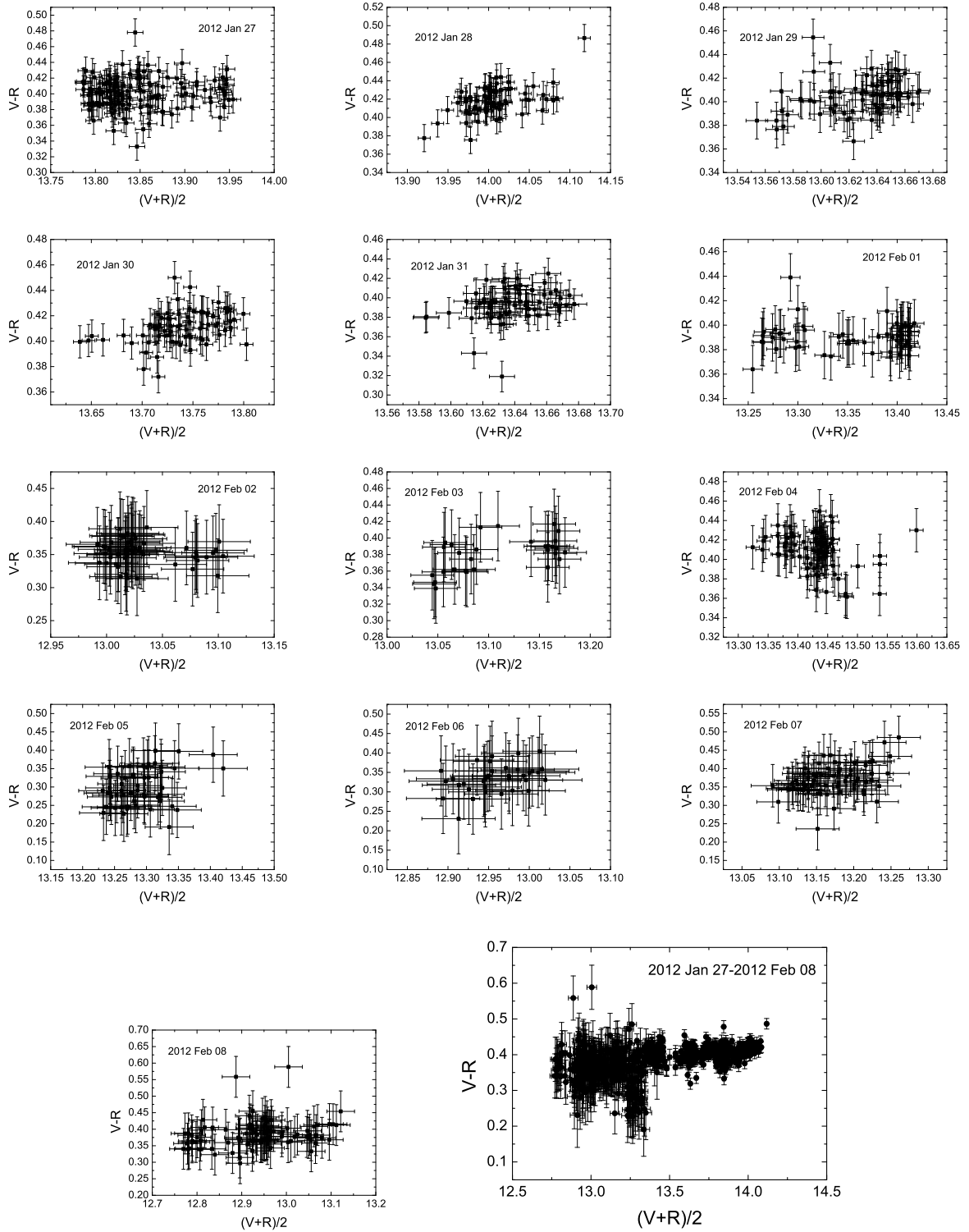


Fig. 6.— The correlations between $V - R$ index and $(V + R)/2$ magnitude on intraday and short timescales.

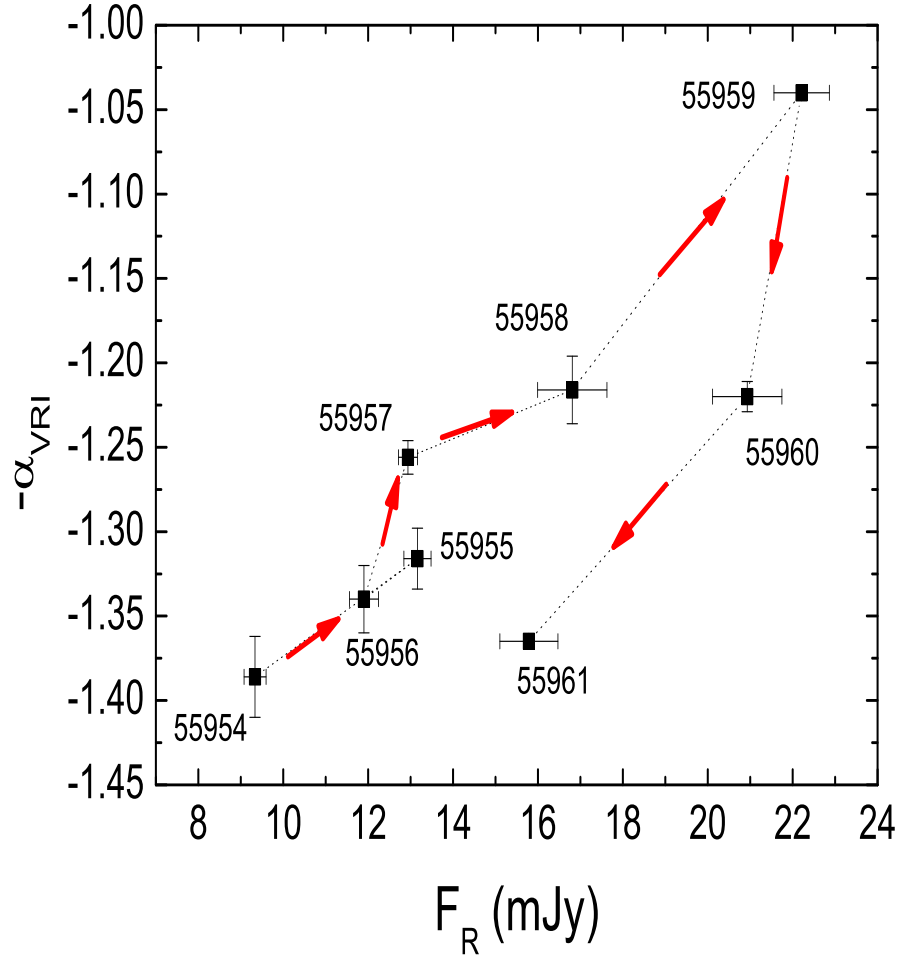


Fig. 7.— The spectral index versus the flux in the flare event. The flare extended from Jan. 28 to Feb. 04.

Table 1. Details of telescopes and instruments.

Telescope	60-cm BOOTES-4
CCD model:	SBIG 1001 E
Chip size:	1024×1024 pixels
Pixel size:	$24.6 \times 24.6 \mu m$
Scale:	$1.07'' \text{ pixel}^{-1}$
Field:	$18' \times 18'$
Gain:	$1.75 e^- \text{ ADU}^{-1}$
Read Out Noise:	$16 e^- \text{ rms}$
Binning used:	1×1
Typical seeing:	1.5 arcsec

Table 2. Observation log of photometric observations

Date(UT)	Band	Number of observations	Time spans(h)	Time resolutions(min)
2012 Jan 27	I	126	6.9	3.2
2012 Jan 27	R	126	6.9	3.2
2012 Jan 27	V	126	6.9	3.2
2012 Jan 27	B	126	6.9	3.2
2012 Jan 28	I	74	7.2	5.9
2012 Jan 28	R	74	7.2	5.9
2012 Jan 28	V	74	7.2	5.6
2012 Jan 28	B	73	7.1	5.9
2012 Jan 29	I	72	7.2	5.9
2012 Jan 29	R	71	7.2	5.9
2012 Jan 29	V	73	7.2	5.9
2012 Jan 29	B	73	7.2	5.9
2012 Jan 30	I	71	6.9	5.9
2012 Jan 30	R	71	6.9	5.9
2012 Jan 30	V	71	6.9	5.9
2012 Jan 30	B	71	6.9	5.9
2012 Jan 31	I	66	6.8	5.9
2012 Jan 31	R	66	6.8	5.9
2012 Jan 31	V	66	6.8	5.9
2012 Jan 31	B	67	6.8	5.9
2012 Feb 01	I	58	5.6	5.9

Table 2—Continued

Date(UT)	Band	Number of observations	Time spans(h)	Time resolutions(min)
2012 Feb 01	R	59	5.7	5.9
2012 Feb 01	V	59	5.7	5.9
2012 Feb 01	B	59	5.7	5.9
2012 Feb 02	I	58	6.8	5.9
2012 Feb 02	R	58	6.8	5.9
2012 Feb 02	V	57	6.6	5.9
2012 Feb 02	B	59	6.8	5.9
2012 Feb 03	I	30	5.1	3.7
2012 Feb 03	R	30	5.1	3.7
2012 Feb 03	V	30	5.1	3.7
2012 Feb 03	B	28	5.0	3.7
2012 Feb 04	I	78	6.2	4.7
2012 Feb 04	R	78	6.2	4.7
2012 Feb 04	V	78	6.2	4.7
2012 Feb 04	B	78	6.2	4.7
2012 Feb 05	I	51	7.2	4.7
2012 Feb 05	R	51	7.2	4.7
2012 Feb 05	V	51	7.1	4.7
2012 Feb 05	B	53	7.0	4.7
2012 Feb 06	I	35	6.4	11.4
2012 Feb 06	R	35	6.4	11.4

Table 2—Continued

Date(UT)	Band	Number of observations	Time spans(h)	Time resolutions(min)
2012 Feb 06	V	35	6.4	11.4
2012 Feb 07	I	66	6.9	4.5
2012 Feb 07	R	67	6.9	4.5
2012 Feb 07	V	65	6.7	4.5
2012 Feb 08	I	94	7.0	4.5
2012 Feb 08	R	94	7.0	4.5
2012 Feb 08	V	93	7.0	4.5

Table 3. Data of B Band

Date(UT)	MJD	Magnitude	σ
2012 Jan 27	55953.6895	14.7430	0.0225
2012 Jan 27	55953.6920	14.7385	0.0225
2012 Jan 27	55953.6943	14.6920	0.0225
2012 Jan 27	55953.6966	14.7290	0.0225
2012 Jan 27	55953.6988	14.7315	0.0225

Note. — Column (1) is the universal time (UT) of observation, column (2) the corresponding modified Julian day (MJD), column (3) the magnitude, column (4) the rms error. Table 3 is available in its entirety in the electronic edition of the *The Astronomical Journal*. A portion is shown here for guidance regarding its form and content.

Table 4. Data of V Band

Date(UT)	MJD	Magnitude	σ
2012 Jan 27	55953.6901	14.2280	0.0133
2012 Jan 27	55953.6924	14.2300	0.0133
2012 Jan 27	55953.6946	14.2095	0.0133
2012 Jan 27	55953.6969	14.2405	0.0133
2012 Jan 27	55953.6992	14.2090	0.0133

Note. — The meaning of each column is the same as that in Table 3. Table 4 is available in its entirety in the electronic edition of the *The Astronomical Journal*. A portion is shown here for guidance regarding its form and content.

Table 5. Data of R Band

Date(UT)	MJD	Magnitude	σ
2012 Jan 27	55953.6904	13.8020	0.0112
2012 Jan 27	55953.6927	13.8100	0.0112
2012 Jan 27	55953.6950	13.8215	0.0112
2012 Jan 27	55953.6973	13.8045	0.0112
2012 Jan 27	55953.6996	13.8015	0.0112

Note. — The meaning of each column is the same as that in Table 3. Table 5 is available in its entirety in the electronic edition of the *The Astronomical Journal*. A portion is shown here for guidance regarding its form and content.

Table 6. Data of *I* Band

Date(UT)	MJD	Magnitude	σ
2012 Jan 27	55953.6908	13.2665	0.0117
2012 Jan 27	55953.6931	13.2760	0.0117
2012 Jan 27	55953.6954	13.2750	0.0117
2012 Jan 27	55953.6976	13.2590	0.0117
2012 Jan 27	55953.6999	13.2750	0.0117

Note. — The meaning of each column is the same as that in Table 3. Table 6 is available in its entirety in the electronic edition of the *The Astronomical Journal*. A portion is shown here for guidance regarding its form and content.

Table 7. Results of IDV Observations of S5 0716+714

Date	Band	C	F	$F_C(99)$	F_A	$F_A(99)$	V/N	A(%)	Ave(mag)
(1)	(2)	(3)	(4)	(5)	(6)	(7)	(8)	(9)	(10)
2012 Jan 27	I	3.69	13.60	1.53	52.89	1.98	V	17.12	13.18
2012 Jan 27	R	4.25	18.08	1.53	58.32	1.98	V	18.23	13.72
2012 Jan 27	V	3.66	13.38	1.53	36.13	1.98	V	18.10	14.13
2012 Jan 27	B	2.78	7.75	1.53	8.02	1.98	V	27.92	14.63
2012 Jan 28	I	4.00	15.99	1.73	27.60	2.44	V	15.61	13.31
2012 Jan 28	R	3.93	15.46	1.73	48.93	2.44	V	12.85	13.94
2012 Jan 28	V	2.93	8.60	1.73	31.00	2.44	V	25.09	14.30
2012 Jan 28	B	2.73	7.44	1.74	28.37	2.45	V	17.13	14.80
2012 Jan 29	I	1.81	3.33	1.75	5.09	2.45	PV		12.95
2012 Jan 29	R	2.60	6.76	1.75	24.43	2.46	V	13.96	13.43
2012 Jan 29	V	3.06	9.37	1.74	26.68	2.45	V	12.81	13.91
2012 Jan 29	B	2.26	5.12	1.74	14.55	2.45	PV		14.41
2012 Jan 30	I	3.76	14.15	1.75	57.76	2.46	V	13.60	13.06
2012 Jan 30	R	4.43	19.62	1.75	49.74	2.46	V	16.46	13.60
2012 Jan 30	V	3.79	14.33	1.75	42.76	2.46	V	17.16	14.03
2012 Jan 30	B	2.75	7.56	1.75	40.27	2.46	V	18.20	14.52
2012 Jan 31	I	1.86	3.46	1.79	6.01	2.54	PV		12.99
2012 Jan 31	R	1.69	2.85	1.79	6.41	2.54	PV		13.51
2012 Jan 31	V	2.31	5.33	1.79	5.78	2.54	PV		13.92
2012 Jan 31	B	1.82	3.31	1.78	4.85	2.53	PV		14.39
2012 Feb 01	I	6.90	47.66	1.87	164.48	2.66	V	17.07	12.72

Table 7—Continued

Date	Band	C	F	$F_C(99)$	F_A	$F_A(99)$	V/N	A(%)	Ave(mag)
(1)	(2)	(3)	(4)	(5)	(6)	(7)	(8)	(9)	(10)
2012 Feb 01	R	8.26	68.23	1.86	77.19	2.65	V	22.05	13.22
2012 Feb 01	V	4.53	20.54	1.86	123.93	2.65	V	18.06	13.63
2012 Feb 01	B	1.96	3.86	1.86	72.58	2.65	PV		14.11
2012 Feb 02	I	1.36	1.86	1.87	24.90	2.66	PV		12.45
2012 Feb 02	R	1.37	1.87	1.87	11.81	2.66	PV		12.92
2012 Feb 02	V	0.82	0.68	1.88	12.49	2.73	PV		13.30
2012 Feb 02	B	0.77	0.62	1.86	12.21	2.65	PV		13.74
2012 Feb 03	I	2.08	4.33	2.42	22.41	3.90	PV		12.47
2012 Feb 03	R	1.95	3.80	2.42	17.45	3.90	PV		12.99
2012 Feb 03	V	1.68	2.84	2.42	8.02	3.90	PV		13.38
2012 Feb 03	B	1.81	3.26	2.51	3.62	3.99	PV		13.86
2012 Feb 04	I	5.36	28.77	1.71	92.85	2.34	V	19.55	12.74
2012 Feb 04	R	3.64	13.26	1.71	77.16	2.34	V	26.53	13.29
2012 Feb 04	V	2.57	6.62	1.71	30.70	2.34	V	28.24	13.72
2012 Feb 04	B	1.36	1.86	1.71	17.71	2.34	PV		14.20
2012 Feb 05	I	1.25	1.58	1.95	15.88	2.89	PV		12.71
2012 Feb 05	R	1.21	1.49	1.95	7.92	2.89	PV		13.21
2012 Feb 05	V	0.95	0.94	1.95	4.20	2.89	PV		13.52
2012 Feb 05	B	1.43	2.06	1.92	13.76	2.85	PV		14.13
2012 Feb 06	I	0.78	0.61	2.26	1.00	3.53	N		12.40
2012 Feb 06	R	0.90	0.80	2.26	5.29	3.53	PV		12.86

Table 7—Continued

Date	Band	C	F	$F_C(99)$	F_A	$F_A(99)$	V/N	A(%)	Ave(mag)
(1)	(2)	(3)	(4)	(5)	(6)	(7)	(8)	(9)	(10)
2012 Feb 06	V	0.79	0.62	2.26	4.51	3.53	PV		13.21
2012 Feb 07	I	1.22	1.54	1.79	41.82	2.53	PV		12.52
2012 Feb 07	R	1.44	2.07	1.78	15.88	2.53	PV		13.06
2012 Feb 07	V	1.21	1.45	1.76	5.87	2.55	PV		13.44
2012 Feb 08	I	2.74	7.52	1.63	92.30	2.21	V	29.27	12.31
2012 Feb 08	R	2.97	8.84	1.63	110.20	2.21	V	33.22	12.81
2012 Feb 08	V	1.89	3.58	1.63	27.82	2.22	PV		13.21

Note. — Column 1 is the date of observation, column 2 the observed band, column 3 the value of C test, column 4 the average F value, column 5 the critical F value with 99 per cent confidence level, column 6 the F value of ANOVA, column 7 the critical F value of ANOVA with 99 per cent confidence level, column 8 the variability status (V: variable, PV: probable variable, N: non-variable), column 9-10 the variability amplitude and daily average magnitudes respectively.

Table 8. Results of change rate.

Date(UT)	Band	MJD*	Magnitude*	CR(Mag/h)
2012 Jan 27	B	55953.6895	14.743	0.037
		55953.8845	14.517	-0.075
		55953.9619	14.782	
	V	55953.7152	14.248	0.039
		55953.8573	14.066	-0.026
		55953.9668	14.188	
	R	55953.7064	13.825	0.038
		55953.8714	13.642	-0.04
		55953.9671	13.763	
	I	55953.7091	13.291	0.03
		55953.8879	13.119	-0.031
		55953.9744	13.225	
2012 Jan 28	B	55954.6851	14.889	0.034
		55954.8249	14.749	-0.032
		55954.8988	14.828	
	V	55954.6859	14.380	0.037
		55954.8052	14.255	-0.032
		55954.8586	14.322	
	R	55954.6865	13.942	0.031
		55954.8346	13.821	-0.054
		55954.8674	13.882	
	I	55954.6871	13.380	0.029

Table 8—Continued

Date(UT)	Band	MJD*	Magnitude*	CR(Mag/h)
		55954.8352	13.281	
		55954.9049	13.328	
2012 Jan 29	V	55955.6805	13.831	-0.026
		55955.8317	13.960	0.027
		55955.9753	13.842	
	R	55955.6811	13.429	-0.02
		55955.8405	13.534	0.03
		55955.9718	13.434	
2012 Jan 30	B	55956.6878	14.401	-0.044
		55956.8243	14.584	0.021
		55956.9602	14.462	
	V	55956.6886	13.924	-0.042
		55956.8333	14.096	0.032
		55956.9487	13.976	
	R	55956.6892	13.506	-0.038
		55956.8298	13.671	0.025
		55956.9657	13.569	
	I	55956.6898	12.975	-0.032
		55956.8345	13.111	0.024
		55956.9745	13.013	
2012 Feb 01	V	55958.8348	13.694	0.054
		55958.9539	13.522	

Table 8—Continued

Date(UT)	Band	MJD*	Magnitude*	CR(Mag/h)
2012 Feb 04	R	55958.8313	13.285	0.052
		55958.9586	13.136	
	I	55958.8319	12.773	0.043
		55958.9798	12.607	
	V	55961.7198	13.616	-0.019
		55961.9772	13.899	
	R	55961.7205	13.185	-0.024
		55961.9778	13.451	
2012 Feb 08	I	55961.7211	12.636	-0.027
		55961.9718	12.868	
	R	55965.6871	12.979	0.039
		55965.9327	12.654	
	I	55965.6911	12.457	0.034
		55965.9430	12.162	

Note. — The ‘*’ stands for increasing/decreasing time points and corresponding magnitudes; When calculating the change rate, we consider the coefficients of correlation > 0.7 ; for the CR, the positive and negative signs are increasing brightness and decreasing brightness respectively.

Table 9. Results of Spearman rank analysis.

Date(UT)	N	r	P
2012 Jan 27	126	0.036	0.69
2012 Jan 28	70	0.38	0.001
2012 Jan 29	69	0.38	0.001
2012 Jan 30	71	0.43	0.0002
2012 Jan 31	66	0.25	0.04
2012 Feb 01	57	0.14	0.32
2012 Feb 02	56	-0.05	0.73
2012 Feb 03	30	0.53	0.002
2012 Feb 04	77	-0.27	0.02
2012 Feb 05	51	0.25	0.07
2012 Feb 06	35	0.41	0.01
2012 Feb 07	65	0.36	0.003
2012 Feb 08	92	0.29	0.006
2012 Jan 28-Feb 08	866	0.56	1×10^{-6}

Note. — N is number of data; r is the coefficient of correlation; P is the significance level.